Photoejection turns non-covalent fluorescent tags into negative reversible photoswitchers

Yuriy Shpinov,[1,†,*] Mrinal Mandal,[1,†,*] Vincent van Deuren,[3] Alienor Lahlou,[1,4] Matthias Le Bec,[1] Raja Chouket,[1] Chaima Hadj Moussa,[1] Clara Bonin,[1] Hessam Sepasi Tehrani,[1] Ian Coghill,[1] Lina El Hajji,[1] Karim Ounoughi,[1] Jaime Franco Pinto,[1] Marie-Aude Plamont,[1] Philippe Pelupessy,[1] Isabel Ayala,[2] Franck Perez,[5] Isabelle Aujard,[1] Thomas Le Saux,[1] Arnaud Gautier,[1] Peter Dedecker,[3,*] Bernhard Brutscher,[2,*] Ludovic Jullien[1,*]

[1] Chimie Physique et Chimie du Vivant, Département de chimie, École normale supérieure, PSL University, Sorbonne Université, CNRS, Paris, France ; [2] Univ. Grenoble Alpes, CEA, CNRS, Institut de Biologie Structurale, Grenoble, France ; [3] Lab for Nanobiology, Department of Chemistry, KU Leuven, Leuven 3001, Belgium; [4] Sony Computer Science Laboratories, Paris, France ; [5] Institut Curie, Université PSL, CNRS UMR144, Paris, France.

† Co-first authors.

∗ To whom correspondence should be addressed; E-mail: Yuriy.Shpinov@ens.psl.eu, Mrinal.Mandal@ens.psl.eu, peter.dedecker@kuleuven.be, bernhard.brutscher@ibs.fr, Ludovic.Jullien@ens.psl.eu

Abstract

Reversibly photoswitchable fluorophores have enabled a broad range of applications in advanced fluorescence bioimaging. Here, we provide an entirely new class of representatives based on a pair: a biomolecular host and a dark photoisomerizable guest, which becomes bright upon complexation. Hence, we introduce **RSpFAST**, which delivers the first non-covalent chemogenetic reversibly photoswitchable fluorescent proteins from combining photoisomerizable fluorogens with the FAST protein tag. Our experimental strategy involving thermokinetic, photochemical, and structural investigations provides a comprehensive mechanistic and kinetic understanding of **RSpFAST**. Building on this theoretical framework, we demonstrate in both live and fixed cells that **RSpFAST** exhibits an unprecedented dual behavior: a stable and wash-free fluorescent labeling tag turns into a negative reversible photoswitcher by simply lowering the fluorogen concentration and increasing light intensity. In this photoejection-driven kinetic regime, **RSpFAST** is shown to be an efficient marker for dynamic contrast and super-resolution microscopy.

Introduction

For many years, the protein labels of choice consisted of small fluorescent organic labels and genetically encoded fluorescent proteins.[1,2] More recently, hybrid 'chemogenetic' systems that combine the versatility of synthetic fluorophores with the selectivity of genetically encoded systems have enabled additional capabilities and flexibility in applications including fluorescence labeling of proteins[3] and RNA.[4] Multiple chemogenetic frameworks are known, including systems that establish direct covalent bonds between the fluorophores and protein component, and systems that leverage non-covalent interactions and thereby allow reversible labeling when combined with a fluorogen that is non-fluorescent in its unbound state. A particularly notable example arises from combining fluorogens with the Fluorescence-activating and Absorption-Shifting Tag (FAST).[5,6] The monomeric 14-kDa FAST protein labeling system has benefited from the development of a large collection of fluorogens, which generate fluorescent tags exhibiting a wide range of absorption/emission wavelengths[7,8,9,10,11,12] and fluorescence lifetimes.[13,14] Its modular design has also allowed its introduction into derived systems such as biosensors[15,16] and di[17,18]/tri[19]-merizers.

Intensive research efforts have also been dedicated to developing 'smart' labels that yield additional functionality via their photochemical behavior. Reversibly switchable fluorescent proteins (RSFPs),[20,21,22] for example, can be reversibly and controllably switched between fluorescent and non-fluorescent states through irradiation with light of appropriate wavelengths. In doing so, they enable powerful imaging modalities such as sub-diffraction imaging,[23] dynamic labeling,[24] and label[25,26,27] and biosensor[28] multiplexing. However, only a small number of such fluorophores are known, mostly arising from a limited range of

fluorescent proteins. In turn, this has restricted the applications of methods that can leverage their properties.

A number of reports have provided hints that photochromism can occur in non-covalently bound chemogenetic systems. Hence, light-induced fluorescence intensity decay and thermal recovery have been described in the Spinach[29,30] and Broccoli[31] fluorogenic aptamers, and in Y-FAST.[32] However, its applications have only been marginally explored.[29,30,33] In this study, we systematically investigate this behavior with **pFAST**[11] and provide a detailed investigation of its underlying chemical mechanism. In doing so, we develop **RSpFAST**. From combining **pFAST** with reversibly photoswitchable fluorogens, **RSpFAST** forms a novel class of light-responsive, photoswitchable fluorophores and introduces non-covalent reversibly switchable fluorescent proteins (ncRSFPs). In contrast to regular RSFPs, these ncRSFPs exhibit photophysical, photochemical, and thermokinetic features that can be tailored by using the fluorogen concentration and light intensity as control parameters. Hence, **RSpFAST** can behave at will as a regular fluorescent tag or as a negative reversible photoswitcher, which photoconverts from a bright to a dark state. This tunability has been harnessed in live and fixed cells for applications in dynamic contrast and super-resolution microscopy.

Results and discussion

Design and syntheses of the fluorogens. To get access to characterizing experiments necessitating high concentrations, we decided to start out investigation by creating new fluorogens exhibiting higher water solubility than the reported ones. We targeted to lower their pK_a (above 8 for previously reported fluorogens[5,11]) in order to be at least partially ionized at pH 7.4. Thus, we synthesized five fluorogens bearing a rhodanine headgroup and the 4-hydroxy-benzylidene motif grafted with one or two electron-withdrawing functional groups (Figure 1a and SI section 2.1): **HBR3Cl**,[11,34] **HBR3CN**, **HBR3Cl5F**, **HBR35DF**, and **HBR3F5OM**.

Proton exchange and photophysical properties of the free fluorogens. In line with our expectations, the pK_a of these fluorogens was found to range from 4.8 ± 0.1 to 6.9 ± 0.1 (SI section 3.4). In their deprotonated state at physiological pH, these fluorogens absorb light between 430 to 470 nm and emit very weak fluorescence between 530 to 590 nm (Figure 1b and SI section 3.1). NMR measurements furthermore showed that the fluorogens exhibit only one (*Z*)-stereoisomer in aqueous solution (SI section 3.5).

Photoisomerization of the free fluorogens. We next probed the photochemistry of these molecules by subjecting solutions to irradiation at 405 or 480 nm, observing fluorescence changes that could satisfactorily be modeled using a two-state model (SI sections 1.1 and 3.2). We determined the cross sections of the associated photochemistry (sum of the cross sections for the forward and inverse transitions) at a high 10^3 $m^2.mol^{-1}$ range for 405 and 480 nm excitation. Full dark recovery of the original state was observed post-irradiation with time constants ranging from 0.38 s for **HBR3F5OM** to more than 1 h for **HBR3CN** (SI section 3.3). Reproducing this series of experiments at several pH allowed us to extract the pK_a of the formed photoproduct for **HBR3Cl**, **HBR3Cl5F**, and **HBR35DF** (SI section 3.4), which was found higher by up to two units compared to that of the thermodynamically stable state.

We next turned to Light-NMR experiments[35] to better understand the observed photochemistry, adopting an illumination geometry that permits homogeneous illumination of the full NMR sample volume.[36] Based on the ^{1}H- and ^{19}F-NMR spectra recorded under constant 405 or 480 nm light at various intensities (SI section 3.5), we confirmed that we were indeed observing (*Z*)-(*E*) photoisomerization, including retrieval of the cross sections associated with both forward and reverse transitions. We also found that the maximal extent of fluorogen photoisomerization using illumination at 405 and 480 nm ranges from 43 to 57 % and from 25 to 29 % respectively.

*The fluorogens exhibit high affinity for **pFAST***. All of the synthesized fluorogens formed complexes with **pFAST** in solution, evidenced by (i) a few tens of nanometer red and blue shift of the fluorogen absorption and emission wavelengths respectively; (ii) a significant enhancement of the fluorogen brightness by more than a factor 100, reaching up to 13000 $M^{-1}cm^{-1}$ for **HBR3F5OM** (Figure 1b, SI section 4.1, and Table S5). We then

titrated 10 nM **pFAST** with a 100 nM fluorogen solution (Figure 1c and SI section 4.2), allowing us to establish the dissociation constants K_d of the **pFAST**-fluorogen complexes (Figure 1d and Table S6). The observed values of 0.1-10 nM are significantly lower than the ones of fluorogens with higher pK_a,[5,11] in line with our previous observation that dropping pH increases K_d.[5] Stopped flow experiments allowed us to retrieve the on- and off-rate constants underlying the **pFAST**-fluorogen association (SI section 4.3), finding values in the 5-20×10^7 $M^{-1}s^{-1}$ and 10^{-2}-10^{-1} s^{-1} range, respectively. Hence, in the absence of illumination, **pFAST** and its fluorogen at K_d concentration exchange between their free and bound states with lifetimes up to the 10 to 100 s time range.

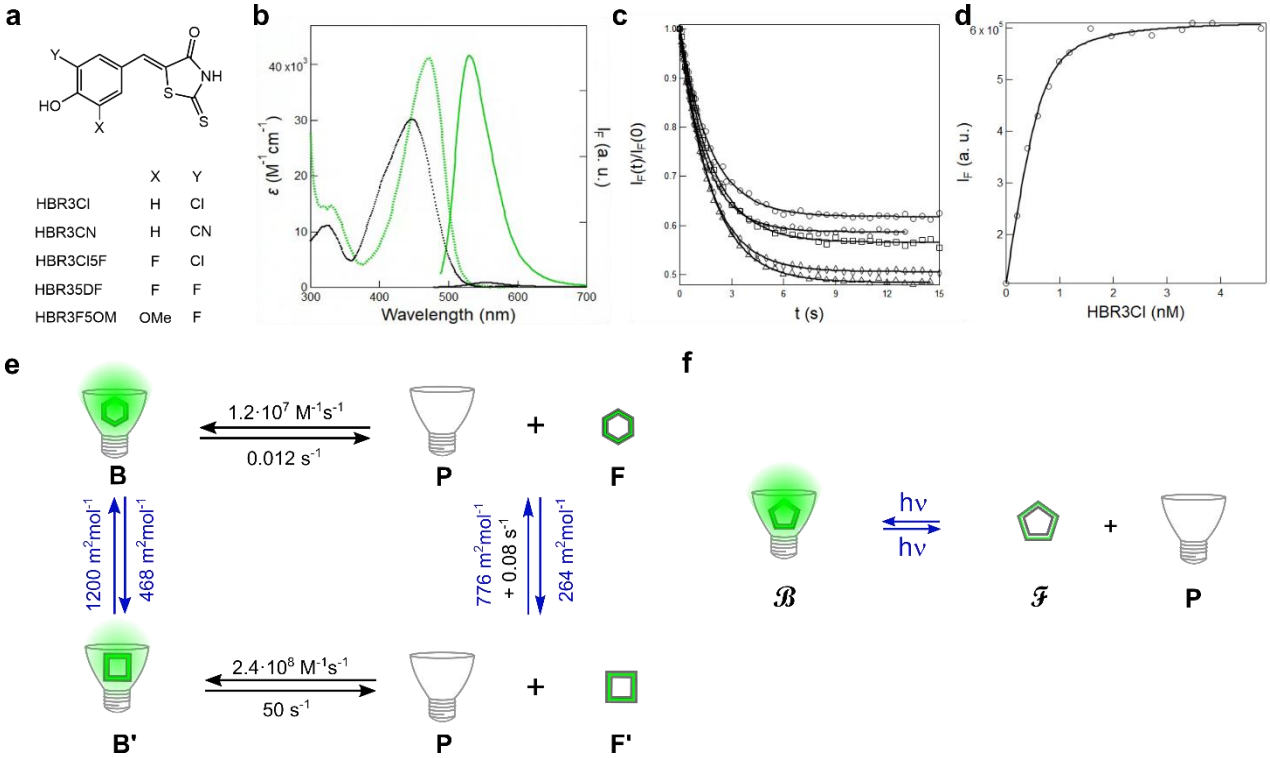

Figure 1. *Reversibly photoisomerizable fluorogens exhibit high affinity for **pFAST***. **a**: Structures of the fluorogens **HBR3Cl**, **HBR3CN**, **HBR3Cl5F**, **HBR35DF**, and **HBR3F5OM**; **b**: Absorption (dotted line) and fluorescence emission (solid line) spectra of **HBR3Cl** (black) and its complex with **pFAST** (green); **c**: Overlay of the fluorescence traces collected at 530 nm normalized by their initial value up to the photostationary state obtained from illuminating 10 nM **pFAST** and **HBR3Cl** at various concentrations (circles, squares, triangles, diamonds and pentagons refer to 0.2, 0.4, 0.6, 2.7, and 7.8 nM respectively) at 480 nm under constant light intensity (1.1×10^{-3} E·m^{-2}·s^{-1}; 2.7×10^{-2} W·cm^{-2}). Markers: Experimental data; solid line: Fit with Eq. (S56); **d**: **HBR3Cl** concentration-dependence of fluorescence intensity at initial time from **c**. Markers: Experimental data at initial time; solid line: Fit with Eq. (S42); **e**: Photocycle of **pFAST-HBR3Cl** (**P** = **pFAST**, **F** = **(*Z*)-HBR3Cl**, **F'** = **(*E*)-HBR3Cl**, **B** = **pFAST-(*Z*)-HBR3Cl**, **B'** = **pFAST-(*E*)-HBR3Cl**) scaled by its rate constants (in M^{-1}·s^{-1} and s^{-1}) and cross sections for photoisomerization (in m^2 mol^{-1}). Its mechanistic reduction in a kinetic regime of photoejection (fluorogen concentration < 1 μM and light intensity > 0.1 E·m^{-2}·s^{-1}; 2.4 W·cm^{-2}) is shown in **f** ($\mathcal{B}$ and $\mathcal{F}$ are the bound and free fluorogen states respectively). Solvent: 10 mM pH 7.4 PBS buffer; T = 293 K.

*The photocycle of the **pFAST**-fluorogen complexes*. Irradiating the **pFAST**-fluorogen complexes with 480 nm light resulted in decays in the fluorescence intensity (Figure 1c and SI section 4.2) that could be reversed in the dark, indicating reversible photochemistry. To investigate this cycle, we performed light jump experiments on highly concentrated solutions of **pFAST** and fluorogens (SI section 4.5). Anticipating the observed photochemistry to be a photoisomerization, we further measured the cross sections associated with the (*Z*)-to-(*E*) and (*E*)-to-(*Z*) **pFAST**-**HBR3Cl** photoisomerization, finding values of 468 m^2.mol^{-1} and 1200 m^2.mol^{-1} at 480 nm. We also found that the ratio of the brightness of the (*E*) and (*Z*) **pFAST**-**HBR3Cl** complexes

is 0.49 respectively, and that the maximal extent of (*Z*)-to-(*E*) photoisomerization in **pFAST-HBR3Cl** is 28 % at 480 nm. The time constant to recover the original fluorescence in the dark was found to range from 33 s for **pFAST-HBR3F5OM** to more than 1 h for the other **pFAST-Fluorogen** complexes (SI section 4.6). These recovery times are much higher than those obtained with the free fluorogens, reflecting much slower thermal back isomerization in the sterically constrained **pFAST** protein cavity.

We next aimed to establish the thermodynamic dissociation constant of the **pFAST-(*E*) Fluorogen** complex by analyzing the dependence between the rate constant of thermal recovery and the **pFAST** concentration (SI section 4.4 and Table S6). The resulting K_d values were found to be in the 0.1-1 µM range, which is three orders of magnitude higher than those observed for the **(*Z*) Fluorogens**. To better investigate this, we exposed **pFAST-(*Z*) Fluorogen** complexes to intense 488 nm illumination, leading to a biexponential drop of the fluorescence signal. The shortest characteristic time showed an inverse dependence on the light intensity, consistent with a photochemical step occurring within the **pFAST** cavity. The longest characteristic time constant, in contrast, did not depend on the light intensity, consistent with a thermally-driven process that we identified as the disruption of the **pFAST-(*E*) Fluorogen** complex (SI section 4.8). Figure 1e summarizes the full thermokinetic characterization of the **pFAST-HBR3Cl** photocycle resulting from the preceding experiments.

*The **pFAST**-fluorogen complexes experience photoisomerization.* We revealed the molecular basis of this photocycle in more detail by solution NMR experiments on a sample of 200 µM uniformly $^{13}C/^{15}N$-labeled **pFAST** and ca. 180 µM of **HBR3Cl**. A ^{1}H-^{15}N correlation spectrum acquired in the dark showed that 90 % of the **pFAST** was bound to **HBR3Cl**, with 10 % remaining as apo **pFAST**. This result was in line with the low **pFAST-HBR3Cl** dissociation constant and the high concentrations of both mixture components with 10 % protein excess. All four ^{1}H resonances of **HBR3Cl** were detected and unambiguously assigned to the (*Z*) **HBR3Cl** configuration (see Figure S43).[37]

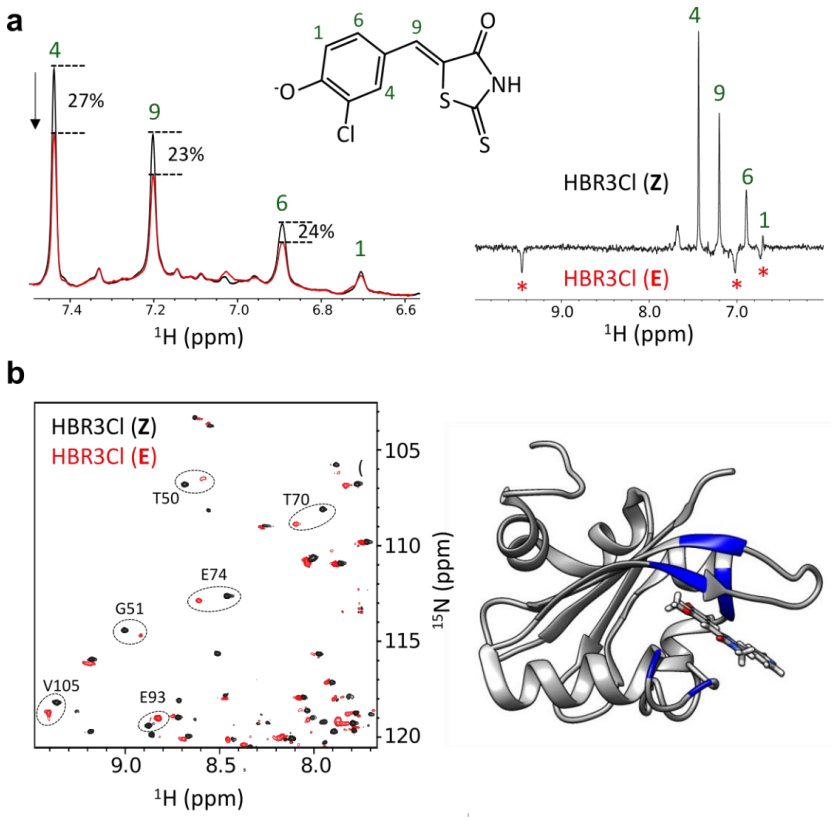

Figure 2. *Solution NMR investigation of the **pFAST-HBR3Cl** complex*. **a**: Superposition of $^{13}C/^{15}N$-filtered ^{1}H NMR spectra (left panel), showing the ^{1}H signals of **HBR3Cl** in the **pFAST-HBR3Cl** complex, recorded for the dark (black lines) and lit (480 nm at 10^{-4} $E.m^{-2}.s^{-1}$ light intensity, 2.5 $mW.cm^{-2}$; red lines) states. The four

detected ^{1}H signals are annotated by the corresponding position in **HBR3Cl**, using the numbering given in the drawing above. A difference spectrum (dark – lit) is plotted in the right panel. The negative signals (marked by red stars) correspond to a new **HBR3Cl** photoproduct in the complex; **b**: ^{1}H-^{15}N difference spectrum (dark-lit), providing a NMR signature of **pFAST** in the dark (black contours) and illuminated (red contours) complex. Only a part of the full spectrum is shown. Amide groups of **pFAST** experiencing large changes of chemical shift between the dark and lit states are highlighted by dashed circles and their corresponding residue number and amino acid type (left panel), and by blue color on the ribbon model representation of a **FAST**-fluorogen complex (right panel). Solvent: 20 mM HEPES buffer at pH 7.5; *T* = 20°C.

We then introduced illumination at 480 nm inside the NMR instrument.[36] After 10 min pre-illumination, we recorded 2D ^{1}H-^{15}N correlation spectra and 1D ^{13}C/^{15}N-filtered ^{1}H spectra of the **pFAST**-**HBR3Cl** complex (Figure 2a). Comparison of the ^{1}H ligand spectra recorded in the dark or under illumination revealed a light-induced intensity drop of the (*Z*) **HBR3Cl** ^{1}H signals by about 25 %, in agreement with the kinetic model shown in Figure 1e that predicts 28 % photoisomerization of bound ligand under these conditions (SI section 1.2.3). The precise nature of this intensity drop could be assessed by computing the difference spectrum (dark – lit) (Figure 2a), which revealed three new ^{1}H ligand signals with negative intensity that provide an NMR signature of the photoproduct. Due to their low signal intensity, we did not perform site-specific resonance assignment. Nevertheless, the new ^{1}H signal detected at 9.4 ppm clearly indicates **HBR3Cl** being in its (*E*) configuration, where one of the ^{1}H (4 or 6) is close to the oxygen atom of the rhodanine heterocycle. Moreover, the intensities of the negative peaks from (*E*)-**HBR3Cl** are significantly lower than the ones of the positive signals from the reduced (*Z*)-**HBR3Cl** population. This indicates NMR line broadening in **pFAST**-**(*E*) HBR3Cl**, most likely caused by the fluorogen dynamics in the protein pocket on the millisecond time scale, in line with an unbinding of (*E*)-**HBR3Cl** in the complex. A ^{1}H-^{15}N difference spectrum (dark – lit) was also computed to identify the **pFAST** amide groups experiencing different chemical environments in the dark and lit states, which are highlighted by blue color on the ribbon model representation of a **FAST-**fluorogen complex structure (PDB 7ava)[38] (Figure 2b). All of the highlighted residues are spatially close to the bound fluorogen, indicating the absence of long-range effects on the **pFAST** structure upon photoisomerization of the **HBR3Cl** ligand. Hence, the NMR experiments demonstrated that the **pFAST**-bound **HBR3Cl** fluorogen is in the (*Z*) configuration in the dark, while illumination promotes formation of its (*E*) configuration, which dissociates more readily on account of its higher K_d for **pFAST**.

*Two kinetic regimes for **RSpFAST**.* The kinetic model of **RSpFAST** obtained by fluorescence spectroscopy and NMR was validated over a wide range of concentrations (nM to mM) and light intensity (10^{-4} to 10^{2} E.m^{-2}.s^{-1}; 2.5×10^{-3} to 2.5×10^{3} W.cm^{-2}). The multiple reactions involved suggest a complex behavior that can yield different observations depending on the experimental conditions. To analyze this more systematically, we computed steady-state phase diagrams of the **pFAST**-**HBR3Cl** complexation as a function of the 480 nm light intensity as well as total concentrations of **pFAST** and **Fluorogen** (Figure S6). Such phase diagrams are key for tailoring the ncRSFPs for applications. Our analysis revealed two distinct kinetic regimes (SI section 1.2):

- In the limit where photoisomerization is slower than binding/unbinding of the fluorogen to **pFAST** (fluorogen concentration > 1 μM and light intensity < 0.1 E·m^{-2}·s^{-1}; 2.4 W.cm^{-2}), the extent of the fluorescence decrease is low, not being more than 28 % for **pFAST**-**HBR3Cl**. This limited contrast arises because the (*E*)-fluorogen is rapidly replaced by a (*Z*)-fluorogen from solution. We call this regime 'photoswitching';

- In the second limit where photoisomerization is faster than binding/unbinding of the fluorogen to **pFAST** (fluorogen concentration < 1 μM and light intensity > 0.1 E·m^{-2}·s^{-1}; 2.4 W.cm^{-2}; Figure 1f), the extent of the achievable fluorescence decrease is much higher, reaching values of 96 % for **pFAST**-**HBR3Cl** under conditions typical for most fluorescence microscopies. This much higher contrast arises because the (*E*)-fluorogen is ejected from **pFAST** (due to its higher dissociation constant) at a faster rate than the recombination of any (*Z*)-fluorogen. We termed this regime 'photo-ejection'.

*Turning **pFAST** into a negative photoswitcher.* We next explored **RSpFAST** as a reversible photoswitcher in the photoejection regime, using **HBR3Cl** and **HBR3F5OM** as the fluorogens. We first imaged live HeLa cells expressing **H2B-pFAST** at the nucleus. The cells were successfully labeled with **HBR3F5OM** solution at a final concentration of 1 μM (Figure 3a), demonstrating that partial fluorogen ionization at neutral pH did not impede its fast permeation through the cell membrane. This fluorescence could be readily suppressed by irradiation at 480 nm (Figure 3b), showing faster fluorescence decreases at higher irradiation intensities (Figure 3c). The original fluorescence level could be recovered by switching off the illumination for 180 s (Figure 3d). Similar fluorescence drop by more than 90 % and thermal recovery was observed on **H2B-pFAST** with 1 μM **HBR3F5OM** in confocal microscopy (Figure 3e), where we tuned the 488 nm light intensity to reach a steady state of fluorogen photoisomerization over the 0.5 μs dwell time duration, and further used 300 ms duration of frame acquisition for photoejection to have enough time to occur between two scans without allowing for extensive recombination of the tag with its fluorogen. Similar results have been obtained with live HeLa cells expressing **Lyn11-pFAST** and **Mito-pFAST** (Figure 1 Extended data), or with **HBR3Cl** with HeLa cells or *Escherichia coli* expressing **H2B-pFAST**, live or after cell fixation (SI Sections 5.2-5.5).

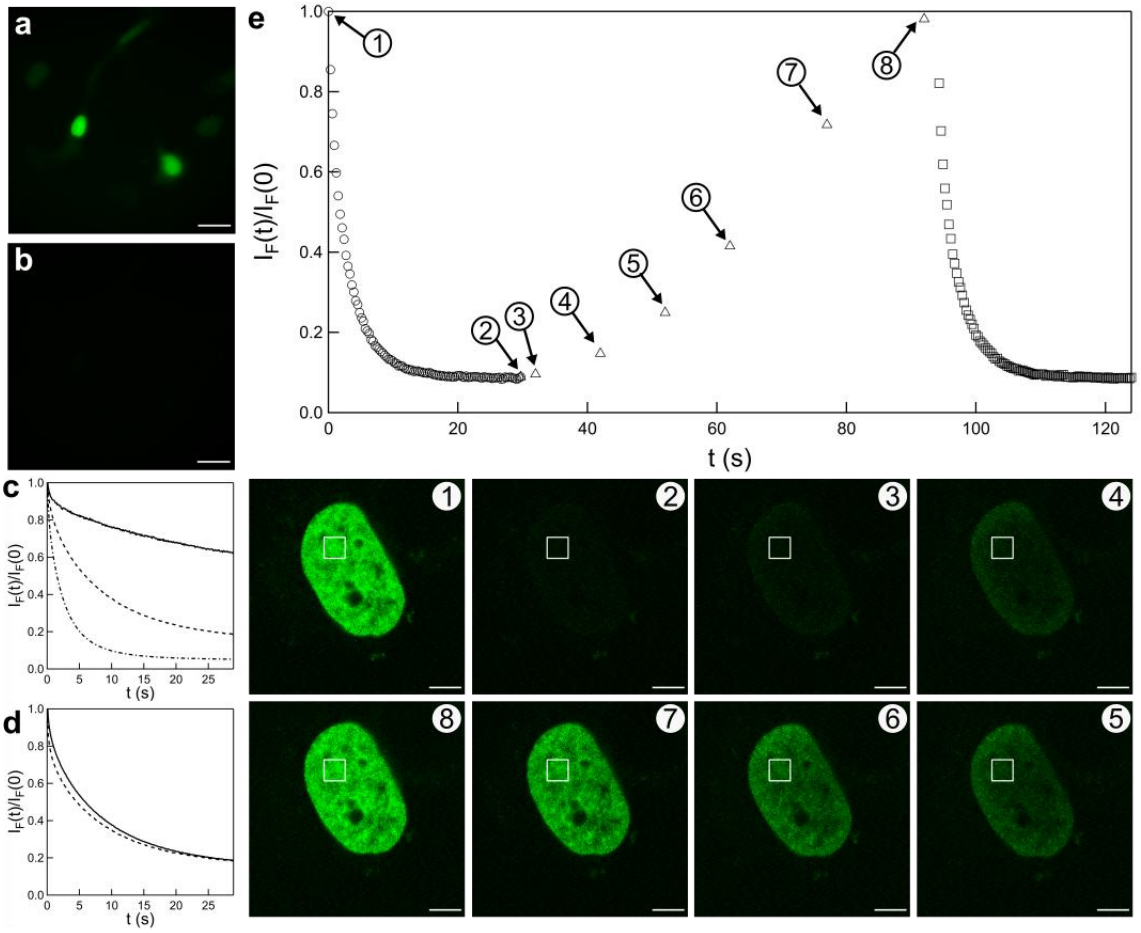

Figure 3. ***pFAST** to generate negative ncRSFPs*. **a**-**d**: 480 (**a**-**d**) or 488 (**e**) nm light-induced photoejection of the **HBR3F5OM** fluorogen in **H2B-pFAST**-labeled live HeLa cells observed in epifluorescence (**a**-**d**) or confocal microscopy (**e**) in the presence of 1 μM fluorogen in DMEM pH 7.4. It is evidenced from the contrast at the nuclei between the initial (**a**,**e1**) and steady state (**b**,**e2**) images quantified at 0.04 (**c**: solid line), 0.43 (**c**: dashed line), and 0.87 (**c**: dashed-dotted line) $E.m^{-2}.s^{-1}$ (resp. 1, 10, and 21 $W.cm^{-2}$) light intensity. Photoejection reversibility is evidenced by the similar loss of fluorescence after two consecutive series of frame acquisition (**d**: 0.43 $E.m^{-2}.s^{-1}$ light intensity, solid line then, after 180 s in the dark, dashed line) or upon varying the delay between two frame acquisitions (**e**: 1.7×10^4 $E.m^{-2}.s^{-1}$, 4.1×10^5 $W.cm^{-2}$ light intensity) in the region of interest at nuclei. Scale bar: 20 μm (for **a**,**b**) and 5 μm (for **e**). See Table S7 for the conditions of image acquisition.

While these results aligned with the proposed photophysical scheme, we noticed that the reduction of the fluorescence level by a factor of ten at steady state in cells was more pronounced than anticipated from the thermokinetic information obtained *in vitro*. Since the recovery of the fluorescence arises through binding of (*Z*)-state of the fluorogen by **pFAST**, a reduced speed of recovery suggests that the free concentration of the fluorogen is lower within cells compared to the bulk medium. In fact, we concluded that the intracellular concentration of free fluorogen available for recombination was in the nanomolar range, amounting to less than 1 % of the extracellular concentration (SI sections 1.3.2.2, 5.1, and 5.5). This presumably reflects binding of the fluorogen to other components within the cell. To our knowledge, this is the first time that a free intracellular fluorogen concentration has been measured directly.

*Dynamic contrast of **RSpFAST** against a spectrally interfering background*. **RSpFAST** photoejection can be used to distinguish its signals from those of a spectrally overlapping but non-photoswitchable background. To illustrate this opportunity, we implemented a correlation method that we recently validated on RSFPs.[39] Figures 4a and 4d display the images of live Hela cells expressing **Lyn11-EGFP** and **H2B-pFAST** in the presence of 1 μM **HBR3F5OM**, showing fluorescence from **EGFP** at the membrane and from **pFAST-HBR3F5OM** at the nucleus. Next, a series of images was acquired during off-switching illumination, allowing the selective extraction of the **pFAST** fluorescence by fitting the observed intensity trajectories to a mono-exponential function (Figures 4b and 4e and SI section 2.6.6). In this way we were able to obtain pure images of the **pFAST-HBR3F5OM** and **EGFP** distributions (Figures 4c and 4f).

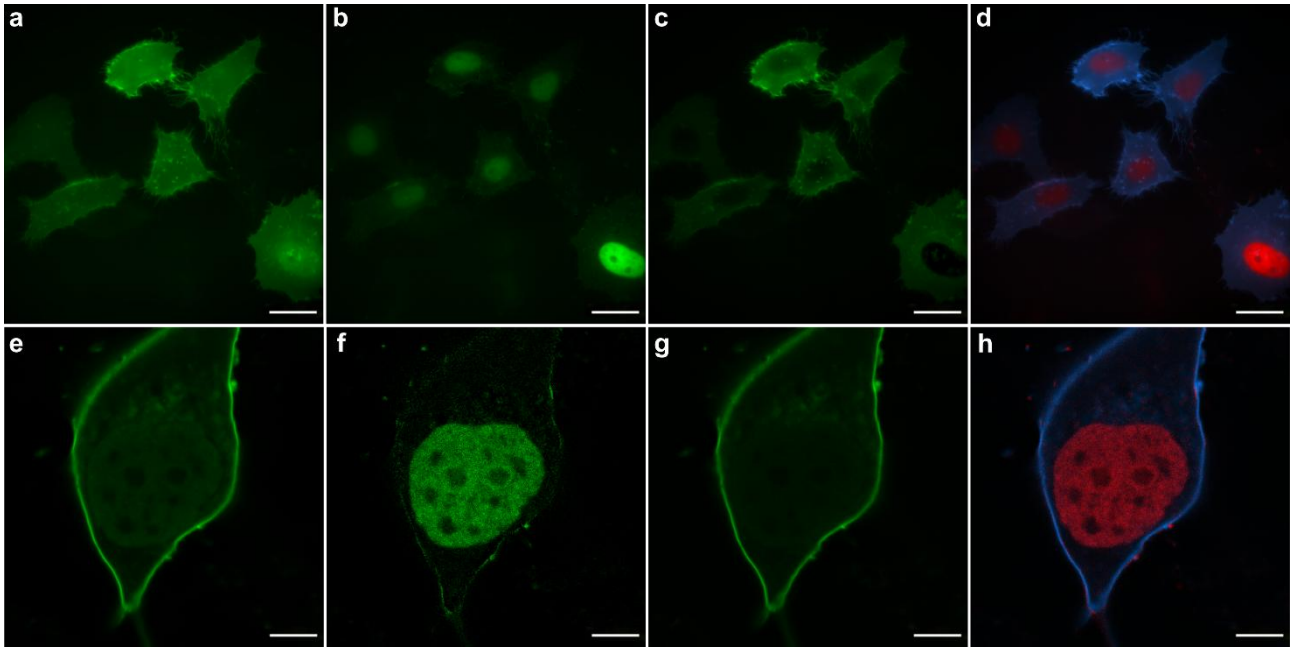

Figure 4. ***RSpFAST** for dynamic contrast against a spectrally interfering background of fluorescence*. **a**,**e**: Epifluorescence (**a**) and confocal (**e**) microscopy image of a live Hela cell expressing **Lyn11-EGFP** and **H2B-pFAST** in the presence of 1 μM **HBR3F5OM**; **b**,**c**,**f**,**g**: Outputs extracted (**b**,**f**) or discarded (**c**,**g**) from correlating the fluorescence time series at each image pixel obtained in **a** and **e** with a monoexponential function associated with the decay time retrieved from monoexponentially fitting the fluorescence decay over the whole field of view in **a** and **e**; **d**,**h**: False color image evidencing **pFAST-HBR3F5OM** (in red) against the spectrally interfering **Lyn11-EGFP** (in blue); scale bar: 20 μm for **a**-**d** and 5 μm for **e**-**h**). See Table S7 for the conditions of image acquisition.

***RSpFAST** photoejection for super-resolution microscopy*. Reversibly photoswitchable fluorophores have found widespread use for super-resolution microscopy and single-molecule localization microscopy.[40] The **FAST** system has also been implemented in this field.[41,42,43] Here, we adopted super-resolution optical fluctuation imaging (SOFI),[44,45] that provides a diffraction-unlimited spatial resolution by correlating

spontaneous single-molecule 'blinking' events and is easily implemented in multiple fluorescence imaging methodologies.

We first acquired single-molecule sensitive fluorescence images at 488 nm of 1 µM **HBR3F5OM**-stained HeLa cells expressing **Lyn11-pFAST** at the plasma membrane (Figure 5a). Pronounced single-molecule intensity fluctuations appeared suitable for SOFI imaging. Indeed, a second-order SOFI analysis confirmed the background rejection and increased spatial information intrinsic to the method,[46] thereby demonstrating **pFAST**:**HBR3F5OM** to be SOFI-compatible.

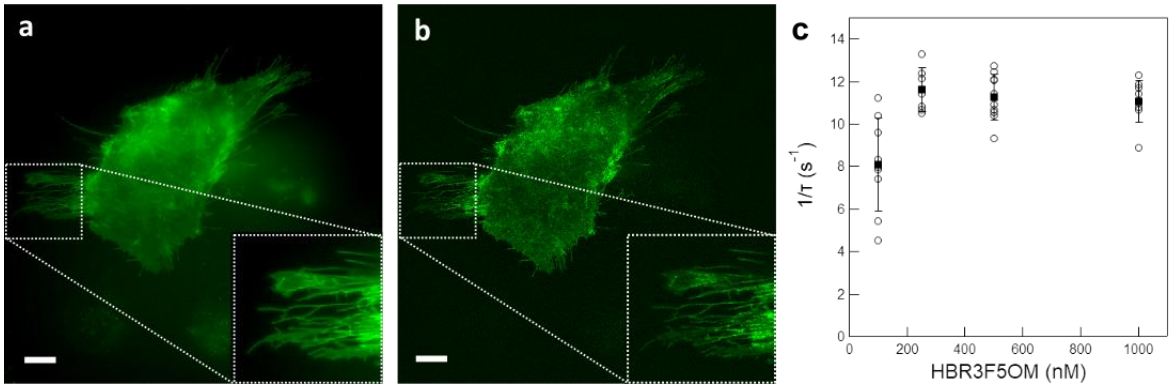

Figure 5. ***pFAST*** *for SOFI*. **a**: Representative averaged wide-field (left) and SOFI (right) images of 1 µM **HBR3F5OM**-labeled **Lyn11-pFAST**-expressing HeLa cells with 25.4×25.4 µm^2 insets acquired at 488 nm light intensity (1.4 E.m^{-2}.s^{-1}; 2.4 mW.cm^{-2}). Scale bar: 10 µm; **b**: Dependence of the inverse of the SOFI decorrelation times on **HBR3F5OM** concentration. Data shows 10 repeats (circles) and average value (square) at each concentration.

SOFI further makes it possible to correlate images separated in time and access the blinking kinetics of the fluorophores. Hence, we calculated SOFI images with different 'lag times' and retrieved the SOFI decorrelation time, identified to the characteristic time of the reduced two-state model in Figure 1f.[47] Figure 5b shows that the dependence of its inverse on the **HBR3F5OM** concentration is weak (see also Figure S52 in SI). In fact, this inverse reports the sum of the rates respectively associated with the disruption of the **pFAST-HBR3F5OM** complex and the recombination between **pFAST** and **HBR3F5OM**, the latter being linearly proportional to **HBR3F5OM** concentration. Considering that **pFAST-(*Z*)-HBR3F5OM** is kinetically inert (25 s lifetime), a thermally-driven exchange between the free fluorogen and its complex would not account for the absence of dependence of the measured characteristic time on **HBR3F5OM** concentration. Hence, we concluded photoejection to govern the exchange observed in SOFI.

Conclusion

In this contribution, we have introduced **RSpFAST**, combining the **pFAST** fluorogen-activating protein with appropriate synthetic chromophores, as a novel class of light-responsive, photoswitchable fluorophores. Through multimodal investigation leveraging fluorescence spectroscopy, NMR experiments, and detailed theoretical modeling, we have developed a quantitative model that discerns not only the chemical species involved, but also the light-induced and thermal reaction rates. We find that photoswitching occurs via cis/trans isomerization of the fluorogen, which can take place both when free in solution and when bound to **pFAST**, altering the observable fluorescence brightness. We measured the affinity of both stereoisomers to **pFAST**, and show that the low-fluorescence (*E*) stereoisomers have a three orders of magnitude reduced affinity, causing dissociation upon isomerization. In the most favorable kinetic regime, we showed that illumination results in accumulation of the free states of the fluorogen thereby strongly depleting its fluorescent bound states. Because the first step in this dissociation process is the light-induced isomerization of the fluorogen, we have named this process 'photoejection'.

To our knowledge, our work is the first to demonstrate and exploit this type of light control within a chemogenetic framework. Reversible photoisomerization has found wide applications in chemistry to shift the extent of bimolecular reactions.[48,49,50,51,52]. To date, the phenomenon observed here was briefly reported in some publications,[29,30] though not fully investigated and not applied to advanced imaging modalities.

Our investigation is notable because of the depth of the chemical model as well as the detailed knowledge and applications that it enables. Compared to more traditional photoswitches, a key feature of **RSpFAST** is the possibility to vary its behavior by changing the fluorogen concentration. In tandem with control over the illumination, we have shown that this results in a range of different behaviors leading to two limiting regimes. When fluorogen association and dissociation is much faster than light-induced fluorogen isomerization, the achievable contrast is limited by the equilibration of the (*E*) and (*Z*) states and their relative brightness. However, when association and dissociation is much slower than light-induced isomerization, the photogenerated (*E*)-stereoisomer dissociates from the **pFAST** moiety and renders it non-fluorescent until a (*Z*)-state fluorogen can be bound. The result is a strong fluorescence contrast between the on- and off-switched states.

Fluorescence recovery (on-switching) does not occur through illumination but rather via the spontaneous fluorogen rebinding, which contrasts with traditional rsFPs in which both transitions are light-controlled. In **RSpFAST** at fluorogen concentrations below the micromolar range, the photoejection regime readily allows off-switching within one second, and left in the dark, the initial bright state recovers after a delay in the range of a few seconds, which makes the **RSpFAST** photocycle relevant for biological timescales.

We further demonstrated that these features make **RSpFAST** an attractive probe for advanced fluorescence imaging. We first showed that it is possible to discriminate the **RSpFAST** fluorescence from that of a spectrally overlapping, but non-photoswitchable fluorophore. Here, **RSpFAST** favorably adds steps of fluorogen association and dissociation to photoswitching mechanisms already present in regular covalent RSFPs, which introduces additional kinetic dimensions to enhance discrimination when implementing dynamic contrast.[26] We also evidenced that **RSpFAST** can deliver super-resolution images. In its easily accessible regime of photoejection, **RSpFAST** benefits from a pilotable exchange between a bright and a completely dark state, which could find other applications, such as reversible FRAP (fluorescence recovery after photobleaching) experiments occurring at fast time scales.[53]

Photoejection as a new regime of photoswitching also allowed us to perform the first measurements of the fluorogen availability inside a cellular environment, which was found to be much lower than expected based on the fluorogen concentration in the medium. In the future, this might allow entirely new assays to be developed. For example, photoejection could be used to gather an idea of the bioavailability of distinct compounds by synthesizing variants intermolecularly coupled to small fluorogens acting as tags, thereby providing direct data on their availability.

In addition to the applications enabled by the current molecules and model, there are several opportunities for future developments. First, all the reported **pFAST** fluorogens exhibit a donor-acceptor molecular structure and are therefore prone to generate ncRSFPs, though this remains to be explored. Furthermore, the current system achieves a limited contrast at high light intensities due to the spectral similarity between the absorption spectra of the (*E*) and (*Z*) stereoisomers. Shifting this equilibrium from 30% to more than 90%, possibly by promoting a spectral blue shift upon photoisomerization like in green RSFPs, would lead to a marked improvement. Eventually, other non-covalent labeling tags that exploit photoisomerizable fluorogens, e.g. Spinach[29,30], may as well show similar ncRSFP behavior.

In summary, we have performed a detailed physicochemical investigation that allowed to propose a novel type of reversible switchable labels based on a chemogenetic scaffold. In current fluorescent microscopies, we found that **RSpFAST** possesses dual functionality of serving both as a simple fluorescence labeling tag and as a negative reversible photoswitcher, the latter being simply obtained by lowering the fluorogen

concentration below a micromolar concentration threshold. This finding opened up key chemical insights as well as the possibility to perform advanced imaging experiments using **RSpFAST** labels. In doing so, our study considerably expands the available tools for advanced fluorescence imaging and sensing.

Acknowledgements

This work was supported by the ANR (ANR-22-CE11-0011). Financial support from the IR INFRANALYTICS FR2054 and the PEPR LUMA for conducting part of this research is gratefully acknowledged.

Author contribution statements

Conceptualization: Y. S., M. M., L. J.; Methodology: Y. S., M. M., L. J.; Software: Y. S., V. v. D., A. L.; Validation: Y. S., M. M., V. v. D., A. L., I. A., T. L. S., A. G., P. D., B. B., L. J. ; Formal analysis: Y. S., M. M., V. v. D., A. L., T. L. S., P. D., B. B., L. J.; Investigation: Y. S., M. M., V. v. D., M. L. B., R. C., C. H. M., C. B., H. S. T., P. P.; Resources: Y. S., M. M., V. v. D., A. L., C. B., I. C., L. E. H., J. F. P., M.-A. P., P. P., I. A.; Data Curation: Y. S., M. M., V. v. D., A. L., P. D., B. B.; Writing - Original Draft: Y. S., M. M., V. v. D., A. L., P. D., B. B., L. J.; Writing - Review & Editing: Y. S., M. M., V. v. D., A. G., P. D., B. B., L. J.; Visualization: Y.S., M. M., V. v. D., A. L., B. B., L. J.; Supervision: F. P., I. A., T. L. S., A. G., P. D., B. B., L. J.; Project administration: L. J.; Funding acquisition: F. P., B. B., L. J.

Competing interests statement

The authors declare competing interests. A patent application has been filed relating to aspects of the work described in this manuscript. Authors listed on the patent: Y. S, M. M., V. v. D., C. B., I. C., L. E. H., J. F. P., F. P., I. A., T. L. S., A. G., P. D., L. J. A.G. and L. J. are co-founder and holds equity in Twinkle Bioscience/The Twinkle Factory, a company commercializing the FAST technology.

Data availability

The datasets generated during and/or analyzed during the current study and that are not in the Supporting Information are available from the corresponding author on request.

Supplementary information

Supplementary information reports on a digest of Theoretical models, Materials and Methods, Investigation of the free fluorogens, Investigation of the **pFAST**-fluorogen complexes, and **RSpFAST** observation in microscopy.

Extended data

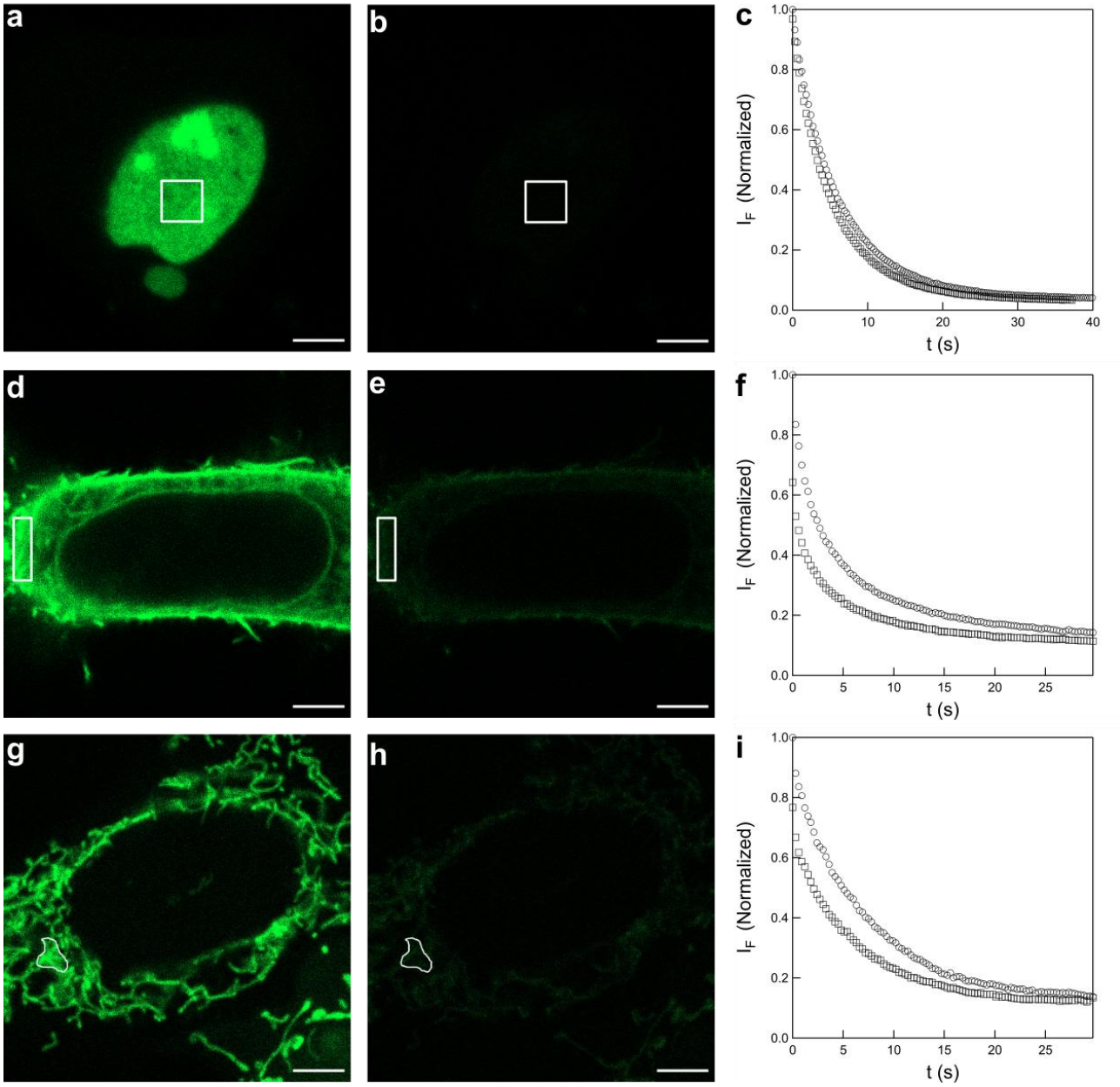

Figure 1 extended data. *pFAST to generate negative ncRSFPs*. 488 nm light-induced photoejections of the **HBR3F5OM** fluorogen in live HeLa cells expressing **H2B-pFAST** (a–c; at the nucleus), **Lyn11-pFAST** (d–f; at the cell membrane), and **Mito-pFAST** (g–i; at mitochondria) observed in confocal microscopy in the presence of 0.1 µM **HBR3F5OM** in DMEM pH=7.4 as evidenced from the contrast between the initial (a,d,g) and steady-state (b,e,h) images quantified at 1.7×10^4 $E\cdot m^{-2}\cdot s^{-1}$, 4.1×10^5 $W.cm^{-2}$ light intensity and checked for reversibility (c,f,i) after two consecutive series of frame acquisition (circles then, after 120 s, squares markers) at 1.7×10^4 $E\cdot m^{-2}\cdot s^{-1}$ light intensity with 0.5 µs dwell time in the region of interest. Scale bar: 5 µm (for a,b,d,e,g,h). T = 293 K.

[1] Wang, L., Frei, M. S., Salim, A., & Johnsson, K. (2018). Small-molecule fluorescent probes for live-cell super-resolution microscopy. Journal of the American Chemical Society, 141(7), 2770-2781.

[2] Rodriguez, E. A., Campbell, R. E., Lin, J. Y., Lin, M. Z., Miyawaki, A., Palmer, A. E., ... & Tsien, R. Y. (2017). The growing and glowing toolbox of fluorescent and photoactive proteins. Trends in biochemical sciences, 42(2), 111-129.

[3] Minoshima, M., Reja, S. I., Hashimoto, R., Iijima, K., & Kikuchi, K. (2024). Hybrid Small-Molecule/Protein Fluorescent Probes. Chemical Reviews, 124(10), 6198-6270.

[4] Neubacher, S., & Hennig, S. (2019). RNA structure and cellular applications of fluorescent light-up aptamers. Angewandte Chemie International Edition, 58(5), 1266-1279.
[5] Plamont, M. A., Billon-Denis, E., Maurin, S., Gauron, C., Pimenta, F. M., Specht, C. G., ... & Gautier, A. (2016). Small fluorescence-activating and absorption-shifting tag for tunable protein imaging in vivo. Proceedings of the national academy of sciences, 113(3), 497-502.
[6] Gautier, A. (2022). Fluorescence-activating and absorption-shifting tags for advanced imaging and biosensing. Accounts of Chemical Research, 55(21), 3125-3135.
[7] Li, C., Plamont, M. A., Sladitschek, H. L., Rodrigues, V., Aujard, I., Neveu, P., ... & Gautier, A. (2017). Dynamic multicolor protein labeling in living cells. Chemical science, 8(8), 5598-5605.
[8] Povarova, N. V., Zaitseva, S. O., Baleeva, N. S., Smirnov, A. Y., Myasnyanko, I. N., Zagudaylova, M. B., ... & Baranov, M. S. (2019). Red-Shifted Substrates for FAST Fluorogen-Activating Protein Based on the GFP-Like Chromophores. Chemistry–A European Journal, 25(41), 9592-9596.
[9] Myasnyanko, I. N., Gavrikov, A. S., Zaitseva, S. O., Smirnov, A. Y., Zaitseva, E. R., Sokolov, A. I., ... & Baranov, M. S. (2021). Color Tuning of Fluorogens for FAST Fluorogen-Activating Protein. Chemistry–A European Journal, 27(12), 3986-3990.
[10] Li, C., Tebo, A. G., Thauvin, M., Plamont, M. A., Volovitch, M., Morin, X., ... & Gautier, A. (2020). A Far-Red Emitting Fluorescent Chemogenetic Reporter for In Vivo Molecular Imaging. Angewandte Chemie International Edition, 59(41), 17917-17923.
[11] Benaissa, H., Ounoughi, K., Aujard, I., Fischer, E., Goïame, R., Nguyen, J., ... & Gautier, A. (2021). Engineering of a fluorescent chemogenetic reporter with tunable color for advanced live-cell imaging. Nature Communications, 12(1), 6989.
[12] El Hajji, L., Bunel, B., Joliot, O., Li, C., Tebo, A. G., Rampon, C., ... & Gautier, A. (2024). A tunable and versatile chemogenetic near infrared fluorescent reporter. bioRxiv, 2024-04.
[13] Bogdanova, Y. A., Solovyev, I. D., Baleeva, N. S., Myasnyanko, I. N., Gorshkova, A. A., Gorbachev, D. A., ... & Baranov, M. S. (2024). Fluorescence lifetime multiplexing with fluorogen activating protein FAST variants. Communications Biology, 7(1), 799.
[14] El Hajji, L., Lam, F., Avtodeeva, M., Benaissa, H., Rampon, C., Volovitch, M., ... & Gautier, A. (2024). Multiplexed In Vivo Imaging with Fluorescence Lifetime-Modulating Tags. Advanced Science, 2404354.
[15] Broch, F., El Hajji, L., Pietrancosta, N., & Gautier, A. (2023). Engineering of Tunable Allosteric-like Fluorogenic Protein Sensors. ACS sensors, 8(10), 3933-3942.
[16] Potekhina, E. S., Bass, D. I., Ezeriņa, D., Fleckenstein, D. D., Chebotarev, A. S., Sysoeva, V. A., ... & Belousov, V. V. (2025). A color-tailored fluorogenic sensor for hydrogen peroxide. Nature Chemical Biology, 1-12.
[17] Tebo, A. G., & Gautier, A. (2019). A split fluorescent reporter with rapid and reversible complementation. Nature communications, 10(1), 2822.
[18] Bottone, S., Joliot, O., Cakil, Z. V., El Hajji, L., Rakotoarison, L. M., Boncompain, G., ... & Gautier, A. (2023). A fluorogenic chemically induced dimerization technology for controlling, imaging and sensing protein proximity. Nature Methods, 20(10), 1553-1562.
[19] Bottone, S., Broch, F., Gedeon, A., Brion, A., El Hajji, L., Benaissa, H., & Gautier, A. (2025). Design and evaluation of a tripartite chemogenetic fluorescent reporter for visualizing ternary protein complexes. Nature Communications, 16(1), 6955.
[20] Nifosì, R., Storti, B., & Bizzarri, R. (2024). Reversibly switchable fluorescent proteins:"the fair switch project". La Rivista del Nuovo Cimento, 1-88.
[21] Bourgeois, D., & Adam, V. (2012). Reversible photoswitching in fluorescent proteins: a mechanistic view. IUBMB life, 64(6), 482-491.
[22] Zhou, X. X., & Lin, M. Z. (2013). Photoswitchable fluorescent proteins: ten years of colorful chemistry and exciting applications. Current opinion in chemical biology, 17(4), 682-690.
[23] Schermelleh, L., Ferrand, A., Huser, T., Eggeling, C., Sauer, M., Biehlmaier, O., & Drummen, G. P. (2019). Super-resolution microscopy demystified. Nature cell biology, 21(1), 72-84.
[24] Ando, R., Mizuno, H., & Miyawaki, A. (2004). Regulated fast nucleocytoplasmic shuttling observed by reversible protein highlighting. Science, 306(5700), 1370-1373.
[25] Quérard, J., Zhang, R., Kelemen, Z., Plamont, M. A., Xie, X., Chouket, R., ... & Jullien, L. (2017). Resonant out-of-phase fluorescence microscopy and remote imaging overcome spectral limitations. Nature communications, 8(1), 969.
[26] Chouket, R., Pellissier-Tanon, A., Lahlou, A., Zhang, R., Kim, D., Plamont, M. A., ... & Jullien, L. (2022). Extra kinetic dimensions for label discrimination. Nature Communications, 13(1), 1482.
[27] Valenta, H., Hugelier, S., Duwé, S., Gerfo, G. L., Müller, M., Dedecker, P., & Vandenberg, W. (2021). Separation of spectrally overlapping fluorophores using intra-exposure excitation modulation. Biophysical Reports, 1(2).
[28] Roebroek, T., Vandenberg, W., Sipieter, F., Hugelier, S., Stove, C., Zhang, J., & Dedecker, P. (2021). Simultaneous readout of multiple FRET pairs using photochromism. Nature Communications, 12(1), 2005.

[29] Wang, P., Querard, J., Maurin, S., Nath, S. S., Le Saux, T., Gautier, A., & Jullien, L. (2013). Photochemical properties of Spinach and its use in selective imaging. Chemical Science, 4(7), 2865-2873.
[30] Han, K. Y., Leslie, B. J., Fei, J., Zhang, J., & Ha, T. (2013). Understanding the photophysics of the spinach–DFHBI RNA aptamer–fluorogen complex to improve live-cell RNA imaging. Journal of the American Chemical Society, 135(50), 19033-19038.
[31] Li, X., Wu, J., & Jaffrey, S. R. (2021). Engineering fluorophore recycling in a fluorogenic RNA aptamer. Angewandte Chemie, 133(45), 24355-24363.
[32] Pimenta, F. M., Chiappetta, G., Le Saux, T., Vinh, J., Jullien, L., & Gautier, A. (2017). Chromophore renewal and fluorogen-binding tags: a match made to last. Scientific Reports, 7(1), 12316.
[33] Pellissier-Tanon, A., Chouket, R., Le Saux, T., Jullien, L., & Lemarchand, A. (2018). Light-assisted dynamic titration: from theory to an experimental protocol. Physical Chemistry Chemical Physics, 20(37), 23998-24010.
[34] Mineev, K. S., Goncharuk, S. A., Goncharuk, M. V., Povarova, N. V., Sokolov, A. I., Baleeva, N. S., ... & Baranov, M. S. (2021). NanoFAST: structure-based design of a small fluorogen-activating protein with only 98 amino acids. Chemical science, 12(19), 6719-6725.
[35] Nitschke, P., Lokesh, N., & Gschwind, R. M. (2019). Combination of illumination and high resolution NMR spectroscopy: Key features and practical aspects, photochemical applications, and new concepts. Progress in Nuclear Magnetic Resonance Spectroscopy, 114, 86-134.
[36] Shpinov, Y., Coghill, I., Mandal, M., Pelupessy, P., Aujard, I., Saux, T. L., & Jullien, L. (2025). A Modular Low-Cost 3D Uniformly Illuminated Mini-Photoreactor with Versatile In-Situ Analysis. Advanced Optical Materials, 13(14), 2403466.
[37] Solyom, Z., Schwarten, M., Geist, L., Konrat, R., Willbold, D., & Brutscher, B. (2013). BEST-TROSY experiments for time-efficient sequential resonance assignment of large disordered proteins. Journal of biomolecular NMR, 55(4), 311-321.
[38] Mineev, K. S., Goncharuk, S. A., Goncharuk, M. V., Povarova, N. V., Sokolov, A. I., Baleeva, N. S., ... & Baranov, M. S. (2021). NanoFAST: structure-based design of a small fluorogen-activating protein with only 98 amino acids. Chemical science, 12(19), 6719-6725.
[39] Pellissier-Tanon, A., Adelizzi, B., Jullien, L., Le Saux, T., & Lemarchand, A. (2022). Correlation of fluorescence evolution for quantitative analysis of labels and sensors. Analytica Chimica Acta, 1225, 340180.
[40] Li, H., & Vaughan, J. C. (2018). Switchable fluorophores for single-molecule localization microscopy. Chemical reviews, 118(18), 9412-9454.
[41] Venkatachalapathy, M., Belapurkar, V., Jose, M., Gautier, A., & Nair, D. (2019). Live cell super resolution imaging by radial fluctuations using fluorogen binding tags. Nanoscale, 11(8), 3626-3632.
[42] Tebo, A. G., Moeyaert, B., Thauvin, M., Carlon-Andres, I., Böken, D., Volovitch, M., ... & Gautier, A. (2021). Orthogonal fluorescent chemogenetic reporters for multicolor imaging. Nature chemical biology, 17(1), 30-38.
[43] Kozma, E., Szatmári, Á., Novák, T., Török, G., Nikić-Spiegel, I., Kormos, A., ... & Kele, P. (2025). Toward Far-red Emitting Chemogenetic Labelling for Live Cell Super-Resolution Microscopy using Fluorescence-Activating and Absorption-Shifting Tag, https://doi.org/10.26434/chemrxiv-2025-k7vd4.
[44] Dedecker, P., Mo, G. C., Dertinger, T., & Zhang, J. (2012). Widely accessible method for superresolution fluorescence imaging of living systems. Proceedings of the National Academy of Sciences, 109(27), 10909-10914.
[45] Moeyaert, B., & Dedecker, P. (2014). PcSOFI as a smart label-based superresolution microscopy technique. In Photoswitching Proteins: Methods and Protocols (pp. 261-276). New York, NY: Springer New York.
[46] Vandenberg, W., Leutenegger, M., Duwé, S., & Dedecker, P. (2019). An extended quantitative model for super-resolution optical fluctuation imaging (SOFI). Optics Express, 27(18), 25749-25766.
[47] Duwé, S., Vandenberg, W., & Dedecker, P. (2017). Live-cell monochromatic dual-label sub-diffraction microscopy by mt-pcSOFI. Chemical Communications, 53(53), 7242-7245.
[48] Emond, M., Le Saux, T., Maurin, S., Baudin, J. B., Plasson, R., & Jullien, L. (2010). 2-Hydroxyazobenzenes to Tailor pH Pulses and Oscillations with Light. Chemistry–A European Journal, 16(29), 8822-8831.
[49] Emond, M., Sun, J., Grégoire, J., Maurin, S., Tribet, C., & Jullien, L. (2011). Photoinduced pH drops in water. Physical Chemistry Chemical Physics, 13(14), 6493-6499.
[50] Liao, Y. (2022). Reversible photo control of proton chemistry. Physical Chemistry Chemical Physics, 24(7), 4116-4124.
[51] Martin, M. M., Plaza, P., Meyer, Y. H., Begin, L., Bourson, J., & Valeur, B. (1994). A new concept of photogeneration of cations: Evidence for photoejection of Ca^{2+} and Li^{+} from complexes with a crown-ether-linked merocyanine by picosecond spectroscopy. Journal of Fluorescence, 4, 271-273.
[52] Adelizzi, B., Gielen, V., Le Saux, T., Dedecker, P., & Jullien, L. (2021). Quantitative model for reversibly photoswitchable sensors. ACS sensors, 6(3), 1157-1165.
[53] Valenta, H., Dalla Vecchia, M., Van den Eynde, R., Vandenberg, W., & Dedecker, P. (2025). Super-resolved Imaging of Molecular Interactions Using FRET-SOFI. Nano Letters.